Combining finite volume and finite element methods to simulate fluid flow in geologic media

Sebastian Geiger* Stephen Roberts†
Stephan K. Matthäi‡ Christopher Zoppou§

(Received 1 June 2001; revised 23rd October 2002)

Abstract

The permeability, porosity, and fluid velocities that govern the flow of multi-phase fluids such as water, oil and

*Department of Earth Sciences, Swiss Federal Institute of Technology (ETH), Sonneggstr. 5, CH-8092 Zurich, Switzerland.
mailto:geiger@erdw.ethz.ch

†Department of Mathematics, Mathematical Sciences Institute, Australian National University, Canberra, ACT 0200, Australia.
mailto:stephen.roberts@anu.edu.au

‡TH Huxley School of Environment, Earth Science and Engineering, Imperial College, RSM Building, Prince Consort Road, London SW7 2BP, England. mailto:s.matthai@ic.ac.uk

§Geosciences Australia, Urban Geosciences, GPO Box 378, Canberra, ACT 2601, Australia. mailto:Christopher.Zoppou@agso.gov.au

[0]See http://anziamj.austms.org.au/V44/CTAC2001/Geig for this article,
 Published 1 April 2003. ISSN 1446-8735

steam in the earth's subsurface often vary over several orders of magnitude and the scales of interest vary from centimetres to kilometres. We describe a node-centred finite volume method coupled with a finite element method on an unstructured triangular grid to accurately and efficiently model multi-phase flow in geologic media. This is demonstrated by modelling multi-phase flows in complex geometries and with transport parameters that vary over several orders of magnitude.

Contents

1 Introduction

Modelling the flow of multi-phase fluids [13] such as water, oil, and steam in the earth's crust is very challenging, since the hydrological

properties, permeability, porosity and fluid velocities in the earth's subsurface vary over many orders of magnitude. As a result, hydraulic conditions often focus fluid flows in large scale fluid reservoirs into structures, such as fractures, of much smaller scale. In such cases the scale of interest varies from the kilometre scale down to the centimetre scale [17, 18].

The combination of finite element and finite volume methods (hereafter called the Combined Element Volume Method (CEVM)) to model multi-phase flow in geologic media has recently become popular [3, 5, 6, e.g.]. These studies have shown that CEVM simulations yield very good results in comparison to traditional finite difference or finite element methods [10]. The CEVM is commonly embedded within an implicit pressure, explicit saturation formulation (IMPES). In the IMPES approach, the fluid pressure field is computed implicitly (here using the finite element method), yielding velocities of the fluid phases which are used to explicitly calculate the mass balance of the fluid phases (here using the finite volume method) [2]. The use of the CEVM and IMPES formulation combines the best features of either method. In particular:

- The geometric flexibility of the finite-element method caters for large variations in scale to be modelled efficiently.
- The non-linear advection equations are decoupled from the parabolic equation for the fluid pressure which avoids the necessity of using a non-linear solver such as Newton's method.
- The parabolic equation for the fluid pressure is solved efficiently by the finite element method and the hyperbolic conservation equation is efficiently solved by the finite volume method.
- Multigrid solvers are employed to solve the equations associated with the finite element method. In particular, algebraic

multigrid methods are used to deal with the large variations in permeability and porosity.

- Mass conservative, total variation diminishing (TVD) finite volume schemes are used to accurately track the propagation of the phase interfaces.

When embedding the CEVM in an IMPES formulation, a mixed-element formulation is commonly used to simultaneously compute the fluid pressure and velocity fields at the finite element nodes [3, 5, 6, 10, e.g.]. This yields a flux that is constant across the faces of the finite elements. This method does not require the construction of a finite volume subgrid. On the other hand, it has the major drawback that the physical solution across interfaces with discontinuous changes of material properties is incorrect [29]. Another disadvantage is that large matrices must be constructed, which increases the storage and CPU time required by the multigrid solvers.

Verma [27] has suggested that the use of node-centred (barycentric) finite volumes is well suited for reservoir simulation. Consider a given finite element mesh, with elements consisting of triangles in two dimensions and a tetrahedrons in three dimensions. In this method, a finite volume subgrid is constructed on the basis of the finite element mesh by connecting the barycentres of the triangles or tetrahedrons with the midpoints of the associated edges (In two dimensions see Figure 1).

In addition to the geometric flexibility of using unstructured meshes, this method has the advantage that only the fluid pressure field need be computed by the finite element method. In contrast to the mixed-element formulation, the transport parameters are now element variables, and element fluid velocities are derived from the fluid pressure field. This leads to a fluid flux that is constant across

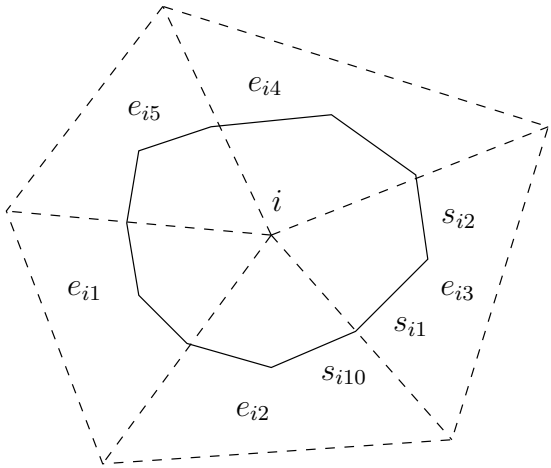

FIGURE 1: Barycentric (node-centered) finite volumes at node i with triangular finite elements e_{i1} – e_{i5} and segments s_{i1} – s_{i10} as defined in [27]

the boundary segments of a finite volume within an associated finite element. Furthermore, with the transport parameters and fluid flux assigned to the finite elements, the contributions of the respective element fluid fluxes are averaged to the nodes conserving the fluid mass within the finite volume. Since the fluid flux can vary from element to element, the formulation can cope with large variations of the transport parameters and discontinuous changes of the material properties.

On the other hand, this formulation requires an expensive construction stage and subsequent storage of a large finite volume subgrid, especially in three dimensions. The feasibility of three different node-centered finite volume discretizations within the CEVM framework were discussed recently [11]. In that study, a mixed-element formulation and nodal transport parameters were used, which can lead to a failure of the algorithm if the mobility tensor becomes negative. The CEVM method is usually applied to the numerical simulation of incompressible fluid phases. Recent studies indicate that CEVM can also be used to model the flow of compressible phases [3, 23].

With CEVM, special attention must be paid to the hyperbolic conservation equation which has the basic form of an advection equation

$$\frac{\partial u}{\partial t} + \nabla \cdot (\mathbf{v}u) = 0 \tag{1}$$

when the dispersive terms are neglected. Here u is the conserved quantity and $\mathbf{v}$ is the velocity vector. Due to its hyperbolic character, solutions of the advection equation are prone to numerical diffusion when using first order methods (e.g., Godunov [7], Lax-Friedrichs [16]) or spurious oscillations when using higher order methods (e.g., Lax-Wendroff [15], Beam-Warming [28]) respectively [30].

Several numerical methods have been developed in recent years that are capable of capturing the advective (shock) front accurately. Popular choices include approximate Riemann solvers [22, 26, e.g.], total variation diminishing (TVD) methods [4, 25, e.g.], essentially non-oscillatory methods (ENO) [8, 24, e.g.], and central schemes [14, 20, e.g.]. While all of these methods have been shown to be robust for numerous applications [1, 31, e.g.], the TVD scheme is the most computationally efficient method when applied to a simple one-dimensional, linear conservation law such as the advection equation. Therefore, the TVD method is usually employed to solve the advection equation within the CEVM framework [3, 5, 6, 10, e.g.].

This paper is structured as follows: In the next section the governing equations for multi-phase flow in geologic media are discussed. This is followed in section 3 by the description of the numerical method, the extension of the TVD method to barycentric finite volumes on unstructured grids. In section 4 we conduct a numerical experiment applying CEVM to a hypothetical example where oil is pumped out of a fractured reservoir.

2 Governing equations

The equations describing the flow of two incompressible and immiscible fluids through geological structures are derived by combining Darcy's law and the individual phase conservation laws [9, e.g.]. Darcy's law provides the following parabolic equation describing the fluid pressure p in the reservoir:

$$\phi c_t \frac{\partial p}{\partial t} = \nabla \cdot [\lambda_t \nabla p] + \frac{1}{2} \nabla \cdot [(\lambda_n - \lambda_w) \nabla p_c] - \mathbf{g} \nabla \cdot [\lambda_n \rho_n + \lambda_w \rho_w] + Q_t \tag{2}$$

where the individual terms will be defined below. Using Darcy's law, the velocity vector $\mathbf{v}_t$ for all fluid phases is then

$$\mathbf{v}_t = -\lambda_t \cdot \nabla p - \frac{1}{2}\left[\lambda_n - \lambda_w\right] \nabla p_c + \mathbf{g}\left[\lambda_n \rho_n + \lambda_w \rho_w\right] . \qquad (3)$$

The average fluid pressure p is given by $(p_w + p_n)/2$ where the fluid pressures of the two phases differ by the capillary pressure $p_c = p_n - p_w$. Furthermore, in equations (2) and (3), ρ_w and ρ_n are the densities of the wetting and non-wetting phase, Q_t is the total fluid volume source or sink given by $Q_t = Q_w + Q_n$, $\mathbf{g}$ is the acceleration due to gravity, ϕ is the porosity of the media, c_t is the compressibility of the fluids and the porous media. The total mobility λ_t and the wetting and non-wetting phase mobilities λ_w and λ_n are

$$\lambda_w = \mathbf{k}\frac{k_{rw}}{\mu_w} , \quad \lambda_n = \mathbf{k}\frac{k_{rn}}{\mu_n} , \quad \lambda_t = \lambda_w + \lambda_n .$$

$\mathbf{k}$ is the permeability of the porous media and k_{rw} and k_{rn} the relative permeability of the wetting and non-wetting phases. These are functions of S_w and can be understood as a scaling factor to the reservoir permeability. The fractional flow function in the wetting phase is

$$f_w = \frac{k_{rw}/\mu_w}{k_{rw}/\mu_w + k_{rn}/\mu_n} .$$

The flow equation describing the conservation of the fluids in the wetting phase in the reservoir is

$$\phi\frac{\partial S_w}{\partial t} = -\nabla \cdot \left[f_w \left(\mathbf{v}_t + \lambda_n \left(\rho_w - \rho_n\right)\mathbf{g}\right)\right] + \nabla \cdot \left[\lambda_n f_w \nabla p_c\right] + Q_w . \qquad (4)$$

where S_w is the phase saturation (that is, volume fraction) of the wetting phase. We need only work with S_w as $S_w + S_n = 1$.

The capillary pressure is usually small compared to the fluid pressure gradient on the reservoir scale [10]. For this reason, in the rest of this paper we neglect capillary effects.

3 Numerical methods

The CEVM numerical method combines a finite volume method to calculate the mass balance of the fluid phases while the fluid pressure field is computed implicitly using the finite element method.

3.1 Finite element method

The finite element method is used to approximate the spatial operators in equation (2) and the backward Euler method is used to discretise the time derivative. This yields the fluid pressure at the nodes of the finite elements at each time step. The nodal fluid pressures are differentiated to compute the total velocities, equation (3), at the centre of the finite elements.

The finite element method (FEM) is a well established numerical method and excellent descriptions of the method are available [12, 29, e.g.]. As such only a brief description is provided here. We use the FEM to approximate the parabolic pressure equation (2).

The computational domain Ω is discretised into a family of triangular finite elements. We also consider a finite element space $\mathbb{V}$ of continuous functions whose restriction to each triangle in the finite element mesh is a polynomial. Usually we consider piecewise constant, linear, quadratic, and cubic functions. For each such FEM space there is a set of m Lagrange points $\mathcal{N}_h = \{\mathbf{x}_i\}_{i=1}^m$ and a set of basis functions $\{\Phi_i\}_{i=1}^m \subset \mathbb{V}$ such that

$$\Phi_i(\mathbf{x}_j) = \begin{cases} 1\,, & \text{if } i = j\,, \\ 0\,, & \text{otherwise.} \end{cases} \tag{5}$$

Then any $v \in \mathbb{V}$ can be written as

$$v(\mathbf{x}) = \sum_{j=1}^{M} v(\mathbf{x}_j)\Phi_j(\mathbf{x})\,. \tag{6}$$

Consider a general differential equation

$$L[u] = 0 \tag{7}$$

where L is a spatial differential operator, for instance Δ. The FEM approximation to the solution of this equation is obtained as the function $u \in \mathbb{V}$ which satisfies

$$\int_\Omega L[u]\ \Phi_i\ d\mathbf{x} = 0 \tag{8}$$

for all basis functions Φ_i. This leads to a set of m (possibly non-linear) equations which need to be solved for the coordinates of u in the given basis $\{\Phi_i\}_{i=1}^m$.

The FEM approximation of equation (2) is given by a function $p(x,t)$ such that $p(\cdot,t) \in \mathbb{V}$ for fixed t. The function p satisfies

$$\begin{aligned}\int_\Omega \phi c_t \frac{\partial p}{\partial t}\Phi_i\ d\mathbf{x} \;&=\; -\int_\Omega \lambda_t \nabla p\cdot\nabla\Phi_i\ d\mathbf{x} \\ &\quad -\int_\Omega (\lambda_n\rho_n + \lambda_w\rho_w)\, g\Phi_i\ d\mathbf{x} + \int_\Omega Q\Phi_i\ d\mathbf{x}\end{aligned} \tag{9}$$

for all basis functions Φ_i. The function p has the decomposition

$$p(\mathbf{x},t) = \sum_{j=1}^{m} p_j(t)\Phi_j(\mathbf{x})\,.$$

In terms of the functions $p_j(t)$, equation (9) is written as the coupled system of ordinary differential equations

$$\sum_{j=1}^{m} \frac{dp_j}{dt}(t)A_{ij}(t) = -\sum_{j=1}^{m} p_j(t)K_{ij}(t) + q_i(t)\,.$$

where

$$A_{ij}(t) = \int_\Omega \phi c_t \Phi_j \Phi_i \, d\mathbf{x}\,, \quad K_{ij}(t) = \int_\Omega \lambda_t \nabla\Phi_j \cdot \nabla\Phi_i \, d\mathbf{x}$$

and

$$q_i(t) = -\int_\Omega \left(\lambda_n \rho_n + \lambda_w \rho_w\right) g \Phi_i d\mathbf{x} + \int_\Omega Q \Phi_i \, d\mathbf{x}\,.$$

Given a time-step Δt, we use a superscript k to denote the approximation of a function at time $k\Delta t$. Then the approximate evolution equation for p_j^k, using backward Euler time stepping, is

$$\sum_{j=1}^{m} (A_{ij}^k + \Delta t\, K_{ij}^k) p_j^{k+1} = \sum_{j=1}^{m} A_{ij}^k p_j^k + \Delta t\, q_i^k\,,$$

which is solved efficiently using algebraic-multigrid methods [21].

3.2 Finite volume method

The elemental velocities given by the fluid pressure field and the relation defined in equation (3) is employed in the finite volume method to compute the mass balance for the fluid phases (equation 4). The finite volumes are centred around the nodes of the finite elements (Figure 1). Integrating equation (4) over a barycentric finite volume V_i and applying the divergence theorem yields

$$\int_{V_i} \phi \frac{\partial S_w}{\partial t} \, dV_i = -\int_{\partial V_i} f_w \left[\mathbf{v}_t + \lambda_n \left(\rho_n - \rho_w\right) g\right] \cdot \mathbf{n} \, dA_i + \int_{V_i} Q_w \, dV_i \tag{10}$$

(neglecting capillary effects). Within each finite volume V_i, the saturation S_w is assumed to be constant. Discretising equation (10)

using Euler's method leads to

$$S_{wi}^{k+1} = S_{wi}^{k} - \frac{\Delta t}{\phi_i |V_i|} \sum_{j=1}^{n_i} \left(f_{wj} \left[\mathbf{v}_{tj} + \lambda_{nj} \left(\rho_{nj} - \rho_{wj} \right) g \right] \right) \cdot \mathbf{n}_j + Q_{wi} \quad (11)$$

where $\sum_{j=1}^{n_i}$ is the summation over all straight line boundary segments j of the finite volume V_i, Δt is the time-step, $|V_i|$ is the area of the control volume and $\mathbf{n}_j$ is the outward normal vector to jth segment, scaled by the length of the segment.

3.2.1 Second-order accuracy and slope limiters

A first-order accurate scheme is obtained if we approximate S_{wi} by a constant for each volume V_i and approximate the fluxes using a simple upwinding scheme. This leads to diffuse and non-physical interfaces between the fluid phases. A higher-order accurate approximation is needed. Second-order accuracy is achieved by computing a gradient of the saturation $\tilde{S}_{wi}$ in the control volume V_i. We use a least squares method to fit a plane through S_{wi} and the saturation values S_{wj} at the n_i neighbouring control volumes V_j of V_i, such that S_{wi} varies linearly in V_i. In two dimensions, the gradient $\mathbf{a} = (a_1, a_2)$ satisfies

$$\sum_{l=1}^{2} M_{kl} a_l = b_k$$

where

$$M_{kl} = \sum_{j=1}^{n_i} (x_{jk} - x_{ik})(x_{jl} - x_{il}) \quad \text{and} \quad b_k = \sum_{j=1}^{n_i} (S_{wj} - S_{wi})(x_{jk} - x_{ik})$$

and x_{i1} and x_{i2} are the two-dimensional spatial coordinates of the centre of mass of finite volume V_i, and x_{j1} and x_{j2} are the spatial

coordinates of the centre of mass of the neighbouring finite volumes V_j. The saturation $\tilde{S}_{wj}$ in the finite volume V_i is computed from

$$\tilde{S}_{wi}(\mathbf{x}) = S_{wi} + \mathbf{a} \cdot (\mathbf{x} - \mathbf{x}_i) \tag{12}$$

where $\mathbf{x} \in V_i$. Using $\tilde{S}_{wi}$, a relation for the relative permeability, the mobility and the fractional flow can be computed at the respective boundary segments of the finite volume, and the finite volume formulation, equation (11) is now solved to second-order accuracy.

Although second-order accuracy is achieved, it is essential to employ a slope limiter to avoid spurious oscillations commonly associated with second-order schemes. In particular the limited function

$$\bar{S}_{wi}(\mathbf{x}) = S_{wi} + \Psi_i \left(\mathbf{a} \cdot (\mathbf{x} - \mathbf{x}_i) \right) \tag{13}$$

where $0 \leq \Psi_i \leq 1$ is a chosen limiter. With $\Psi_i = 0$, the saturation S_{wi} is constant in V_i resulting in a first-order scheme.

We use the MINIMOD limiter

$$\Psi_j = \min \left[r_i, 1 \right] \tag{14}$$

where

$$r_i = \begin{cases} (S_{wi}^{\max} - S_{wi}) / (S_{wj} - S_{wi}) \,, & \text{if } S_{wj} > S_{wi} \,, \\ (S_{wi}^{\min} - S_{wi}) / (S_{wj} - S_{wi}) \,, & \text{if } S_{wj} < S_{wi} \,, \\ 1 \,, & \text{if } S_{wj} = S_{wi} \,, \end{cases}$$

and

$$S_{wi}^{\min} = \min \left(S_{wi}, \min_{j=1,\ldots,n_i} S_{wj} \right) \,, \quad S_{wi}^{\max} = \max \left(S_{wi}, \max_{j=1,\ldots,n_i} S_{wj} \right)$$

the minima and maxima over all neighbouring finite volumes.

4 Two-phase flow in a fractured reservoir

Faults in oil reservoirs have a strong influence on the total permeability of the reservoir and cause difficulties when predicting oil recovery [17, 18]. Two numerical experiments are provided to test the applicability of our method to reservoir simulations. All fractures are 10 cm wide and are represented as thin cuts in a plan view of the reservoir. The oil has a density of $\rho_n = 800.0$ kg m^{-3} and a viscosity of $\mu_n = 5.0 \times 10^{-3}$ Pa s^{-1}. The water, which fills the rest of the pore space, has a density of $\rho_w = 1000.0$ kg m^{-3} and a viscosity of $\mu_w = 1.0 \times 10^{-3}$ Pa s^{-1}. The matrix permeability in the reservoir is set to $\mathbf{k} = 1.0 \times 10^{-13}$ m^2 while the fracture permeability is $\mathbf{k} = 1.0 \times 10^{-9}$ m^2. The matrix porosity is $\phi = 0.1$ while the fracture porosity is $\phi = 1.0$. The water saturation is $S_w = 0.1$ in the reservoir and $S_w = 1.0$ elsewhere. The well is 20 cm in diameter and its casing has a permeability of $\mathbf{k} = 1.0 \times 10^{-10}$ m^2. The pumping rate is 1.16×10^{-4} m^3 s^{-1}. This rate leads to steep pressure gradients such that capillary effects can be neglected.

The following relative permeability relations are used in the simulations

$$k_{rw}(S_n) = 1.0 - 2.7674 S_n + 2.692 S_n^2 - 0.9381 S_n^3$$

and

$$k_{rn}(S_n) = 1.8038 S_n - 2.0551 S_n^2 + 1.243 S_n^3$$

which are least square fits through relative permeability values that were measured in experiments provided by Golder Associates. Our numerical methods are implemented in the object-oriented `C++` code CSP3D3.0 [19].

To study the effects of buoyancy forces, we consider a well with 2 m open casing located above an inclined fracture (Figure 2). The

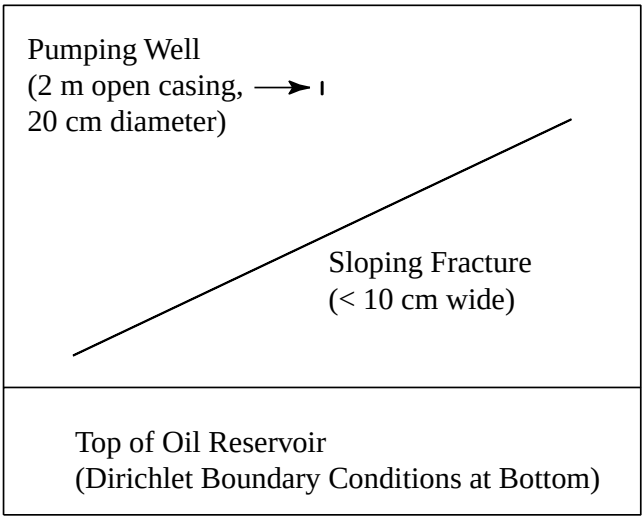

FIGURE 2: Model setup (cross section) for the simulation of pumping of an oil reservoir with an thin, inclined, and highly permeable fracture above the reservoir. Model dimensions are 100×80 metres.

oil reservoir is located underneath the fracture. The saturation at the bottom of the oil reservoir is held constant implying that the oil reservoir extends across the model boundaries. The model dimensions are 100 metres high by 80 metres wide. The unstructured mesh consisted of 9544 finite elements and 4875 finite volumes (8 MB storage requirements for the grids, CPU time on a standard 667 Mhz Pentium III is 8.5 minutes for one time step simulating 10 days of pumping).

The numerical simulation (Figure 3) shows how the inclined fracture disturbs the fluid pressure gradient caused by the pumping. The fluid pressure gradient underneath the fracture is reduced, which forces the oil to rise upwards in distinct fingers. In between the fingers, the denser water sinks down into the oil reservoir. The

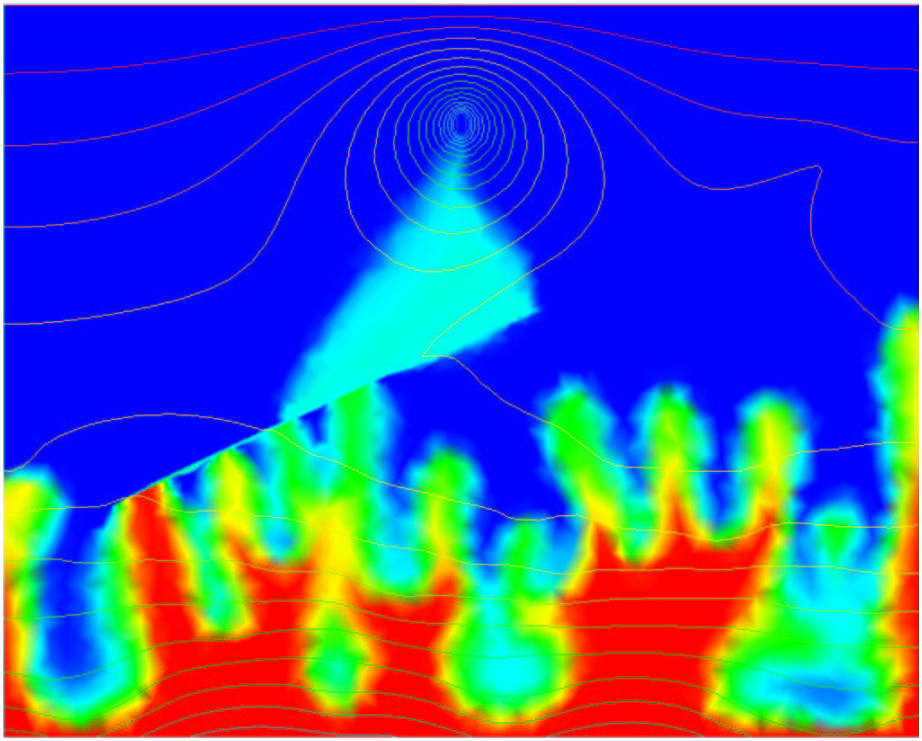

FIGURE 3: Oil saturation (volume fraction) after 2000 days of pumping. Oil saturation is shown in rainbow colour shading (from red=0.9 , to blue=0.0). Contours depict the relative fluid pressure (with buoyancy effects). Note how the fracture and the buoyancy effects disturb the fluid pressure field. The total velocity $\mathbf{v}_t$ varies from 3.6×10^{-12} m s^{-1} to 4.6×10^{-5} m s^{-1} . The oil is then forced into the high permeable fracture from which it is drawn towards the well.

oil fingers displace the water due to the buoyancy effects, because the difference in the fluid densities imposes a stronger fluid pressure gradient underneath the fracture than the pumping. If the buoyancy effects were neglected then the oil would essentially rise uniformly upwards. When the oil reaches the high-permeability fracture, it is forced into the fracture. It migrates along the fracture until it finally departs into the region above the fracture and moves towards the well. Figure 3 shows the oil saturation and relative fluid pressure after 2000 days.

5 Conclusion and outlook

We have described a combined finite element-finite volume method with node-centred finite volumes constructed on a triangular finite element grid. An implicit pressure, explicit saturation solution method is presented. This approach is an efficient way to model two-phase flow of incompressible fluids in geologic media with complex geometrical structures and large variations in the hydrological rock properties (permeability, porosity) and fluid velocities. The node-centred finite volumes do not require the use of a mixed-element formulation to solve for the fluid pressure and fluid velocities simultaneously. Thus, the method can deal with discontinuous changes of the material properties. Furthermore, the construction of large global matrices is avoided, which partly compensates for the storage required by the construction of the finite volume subgrid. However, the storage necessary to construct a 3D finite volume subgrid from tetrahedral elements significantly increases making the method less efficient for 3D simulations. Using higher-order finite volume methods, very accurate numerical solutions can be achieved.

The proposed method is being extended to model the flow of

compressible fluids and to include an equation of state to simulate the flow of miscible fluids (e.g., water and steam) in a variety of geological environments. Capillary pressure relationships will also be included so that capillary effects can be modelled accurately.

References

[1] Ambrosi, D., Corti, S., Pennati, V., and Saleri, F., Numerical simulation of unsteady flow at Po river delta. *Journal of Hydraulic Engineering*, **122**, 735–743, 1996. C186

[2] Aziz, K. and Settari, A., Petroleum Reservoir Simulation. *Applied Science Publishers*, 476 pages, 1979. C182

[3] Bergamaschi, L., Mantica, S., and Manzini, G., A mixed finite element-finite volume formulation of the black-oil model. *SIAM Journal on Scientific Computing*, **20**, 970–997, 1996 C182, C183, C185, C186

[4] Boris, J.P. and Book, D.L., Flux-corrected transport. I. SHASTA, A fluid transport algorithm that works. *Journal of Computational Physics*, **11**, 38–69, 1973. C186

[5] Durlofsky, L.J., A triangle based mixed finite-element-finite volume technique for modeling two phase flow through porous media. *Journal of Computational Physics*, **105**, 252–266, 1993. C182, C183, C186

[6] Eymard, R., Gallouët, T., and Joly, P., Hybrid finite element techniques for oil recovery simulation. *Computer Methods in Applied Mechanics and Engineering*, **74**, 83–98, 1989. C182, C183, C186

[7] Godunov, S.K., The finite difference method for the computation of discontinuous solutions of the equations of fluid dynamics. *Mat. Sb.*, **47**, 357–393, 1959. C185

[8] Harten, A., ENO schemes with subcell resolution. *Journal of Computational Physics*, **83**, 148–184, 1987. C186

[9] Helmig, R., Multi-phase flow and transport processes in the subsurface. *Springer Verlag*, 397 pages, 1997. C186

[10] Huber, R. and Helmig, R., Multi-phase flow in heterogeneous porous media: A classical finite element method versus and implicit pressure-explicit saturation-base mixed finite element-finite volume approach. *International Journal for Numerical Methods in Fluids*, **29**, 899–920, 1999. C182, C183, C186, C187

[11] Huber, R. and Helmig, R., Node-centered finite volume discretizations for the numerical simulation of multi-phase flow in heterogeneous porous media. *Computational Geosciences*, **4**, 141–164, 2001. C185

[12] Huyakorn, P.S. and Pinder, G.F., Computational methods in subsurface flow. *Academic Press*, 473 pages, 1987. C188

[13] Ingebritsen, S.E. and Sanford, W.E., Groundwater in geologic processes, *Cambridge University Press*, 270 pages, 1999. C181

[14] Jiang, G.S. and Tadmor, E., Non-oscillatory central schemes for multidimensional hpyerbolic conservation laws. *SIAM Journal on Scientific Computing*, **19**, 1892–1917, 1998. C186

[15] Lax, P.D. and Wendroff, B., Difference methods with higher order accuracy for solving hyperbolic equations.

Communications on Pure and Applied Mathematics, **17**, 381–398, 1964. C185

[16] Lax, P.D., Weak solutions of nonlinear hyperbolic equations and their numerical computations. *Communications on Pure and Applied Mathematics*, **17**, 159–193, 1954. C185

[17] Matthäi, S.K., and Roberts, S.G., The influence of fault permeability on single phase fluid flow near fault-sand intersections: Results from steady state high-resolution models of pressure-driven fluid flow. *American Association of Petroleum Geologists, Bulletin*, **80**, 1763–1779, 1996. C182, C193

[18] Matthäi, S.K., Aydin, A., Pollard, D.D., and Roberts, S.G., Numerical simulation of departures from radial dradown in a faulted sandstone reservoir with joints and deformation bands. *In:* Jones, G., Fisher, Q.J., and Knipe, R.J., (eds) *Faulting, Fault Sealing and Fluid Flow in Hydrocarbon Reservoirs.* Geological Society, London, Special Publications, **147**, 157–191, 1998. C182, C193

[19] Matthäi, S.K., Geiger, S., and Roberts, S.G., Complex System Platform CSP3D3.0 User's Guide. *Department of Earthsciences, ETH Zurich, Switzerland*, 144 pages, 2001. C193

[20] Nessyahu, H. and Tadmor, E., Non-oscillatory central differencing for hyperbolic conservation laws. *Journal of Computational Physics*, **87**, 408–463, 1988. C186

[21] Roberts, S. and Matthäi, S.K., High Resolution Potential Flow Methods in Oil Exploration. In *Computational Techniques and Applications: CTAC95*, pages 677–684. World Scientific Press, Singapore, 1996. C190

[22] Roe, P.L., Approximate Riemann solvers, parameters vectors, and difference schemes. *Journal of Computational Physics*, **43**, 357–372, 1981. C186

[23] Pain, C.C., Mansoorzadeh, C.R., de Oliveira, E., and Goddard, A.J.H., Numerical modelling of gas-solid fluidized beds using the two-fluid approach. *International Journal for Numerical Methods in Fluids*, **36**, 91–124, 2001. C185

[24] Shu, C.W. and Harten, A., Efficient implementation of essentially non-oscillatory shock capturing schemes. *Journal of Computational Physics*, **77**, 439–471, 1988. C186

[25] Sweby, P.K., High resolution schemes using flux limiters for hyperbolic conservation laws. *SIAM Journal on Numerical Analysis*, **21**, 995–1011, 1984. C186

[26] Toro, E.F., A weighted average flux method for hyperbolic conservation laws. *Proceedings of the Royal Society*, Series A **423**, 401–418, 1989. C186

[27] Verma, S.K., Flexible grids for reservoir simulation. *Ph.D. Thesis Stanford University*, 255 pages, 1996. C183, C184

[28] Warming, R.F. and Beam, R.M., The modified equation approach to the stability and accuracy of finite-difference methods. *Journal of Computational Physics*, **14**, 159–179, 1976. C185

[29] Zienkiewicz, O.C. and Taylor, R.L., The finite element method, 5th Edition. *Butterworth-Heinemann*, Volumes 1–3, 2000. C183, C188

[30] Zoppou, C. and Roberts, S., Behaviour of finite difference schemes for advection diffusion equations. *Mathematics Research Report, The Australian National University,*

Centre for Mathematics and its Applications, **MRR 062-96**, 13 pages, 1996. C185

[31] Zoppou, C. and Roberts, S., Numerical solution of the two-dimensional unsteady dam break. *Applied Mathematical Modelling*, **24**, 457–475, 2000. C186